Journal of Biomolecular NMR **29:** 543–544, 2004.

Letter to the Editor: ^{1}H, ^{13}C, ^{15}N resonance assignments of the cytokine LECT2

Mie Ito[a], Koji Nagata[a,b], Fumiaki Yumoto[a], Satoshi Yamagoe[c], Kazuo Suzuki[c], Kyoko Adachi[d] & Masaru Tanokura[a,*]

[a]*Department of Applied Biological Chemistry, Graduate School of Agricultural and Life Sciences and* [b]*Biotechnology Research Center, The University of Tokyo, 1-1-1 Yayoi, Bunkyo-ku, Tokyo 113-8657, Japan;* [c]*Department of Bioactive Molecules, National Institute of Health, 1-23-1 Toyama, Shinjuku-ku, Tokyo 162-8640, Japan;* [d]*Marine Biotechnology Institute, Heita, Kamaishi, Iwate 026-0001, Japan*

Received 9 February 2004; Accepted 15 March 2004

Key words: cytokine, LECT2, resonance assignments

Biological context

Human LECT2 (leukocyte cell-derived chemotaxin 2) is a 16-kDa chemotactic protein consisting of 133 amino acids and three intramolecular disulfide bonds. The protein was first purified from the culture fluid of phytohemagglutinin-activated human T-cell leukemia SKW-3 cells as a chemotactic factor to human neutrophils (Yamagoe et al., 1996) and its cDNAs were cloned from cDNA libraries of human, bovine, and murine livers (Yamagoe et al., 1998a,b). LECT2 is identical to chondromodulin-II (Hiraki et al., 1996), a bovine protein that stimulates the proliferation of chondrocytes and osteoblasts (Shukunami et al., 1999). A point mutation in LECT2 (Val58 to Ile58) is associated with the severity of rheumatoid arthritis (RA) (Kameoka et al., 2000). No tertiary structure has been solved so far for LECT2 and its related proteins. In order to reveal the three-dimensional structure of LECT2 and the effect of the point mutation on its conformation, we are doing NMR structural analysis of human LECT2. Here we report the ^{1}H, ^{15}N, and ^{13}C resonance assignments.

Methods and experiments

Human LECT2 (the 133-amino acid mature form, residue numbers 19–151) with an N-terminal His_6-tag was produced in *E. coli* as inclusion bodies, and renatured *in vitro* by a three-step refolding procedure (Ito et al., 2003). To prepare stable isotope-labeled protein, $^{15}NH_4Cl$ (> 99% ^{15}N) and ^{13}C-glucose (> 99% ^{13}C) were used as the sole nitrogen and carbon sources, respectively. The samples used for NMR measurements were 1 mM ^{15}N-labeled and $^{13}C/^{15}N$-labeled $(His)_6$-LECT2 dissolved in 50 mM Na_2SO_4 in 85% H_2O/10% D_2O/5% glycerol (pH 6.0, direct meter reading). NMR spectra were recorded at 298 K on Varian Unity Inova NMR spectrometers operated at ^{1}H frequencies of 500- and 750-MHz and equipped with triple-resonance z-gradient probes.

Sequence-specific backbone assignments were elucidated from 3D data of HN(CO)CA, HNCA, CBCA(CO)NH, HNCACB, CBCANH, HNCO, and (HCA)CO(CA)NH. C(CO)NH was used to confirm amino-acid types. For side-chain ^{1}H assignments, H(CCO)NH, HCCH-TOCSY, HCCH-COSY, ^{15}N-edited TOCSY, ^{15}N-edited NOESY, and 2D NOESY were used. ^{1}H chemical shifts were directly referenced to the resonance of 2,2-dimethyl-2-silapentane-5-sulfonate (DSS), while ^{13}C and ^{15}N chemical shifts were referenced indirectly to DSS (Wishart et al., 1995). NMR data were processed using NMRPipe/NMRDraw (Delaglio et al., 1996). Visualization of transformed data and peak-picking were carried out using Sparky (http://www.cgl.ucsf.edu/home/sparky/). Secondary structure was predicted using CSI (Wishart and Sykes, 1994).

*To whom correspondence should be addressed. E-mail: amtanok@mail.ecc.u-tokyo.ac.jp

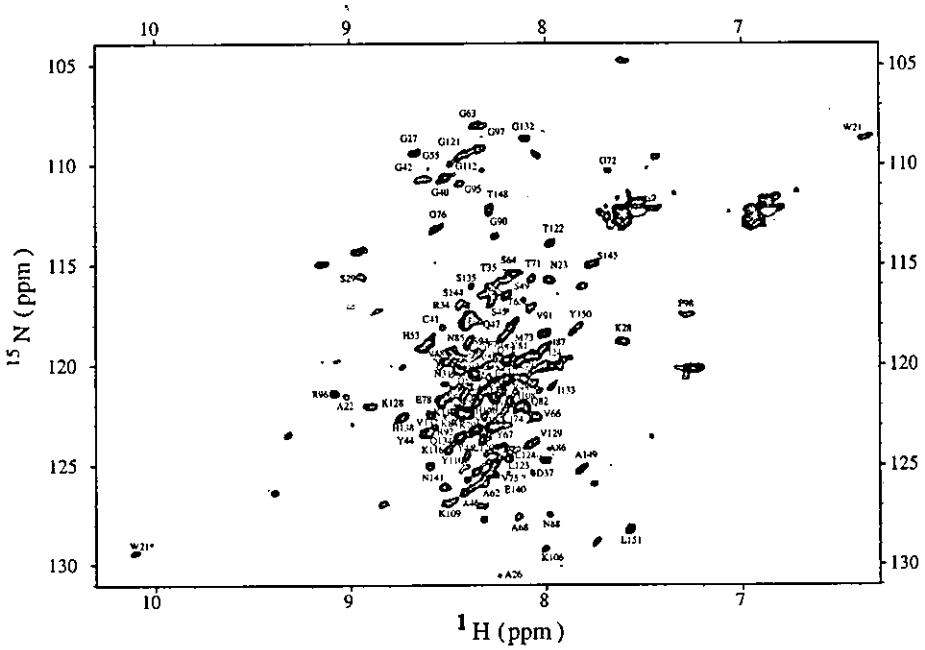

Figure 1. ^{1}H-^{15}N HSQC spectrum of $(His)_6$-LECT2 at 298 K. Amino acid labels were omitted from the middle of the HSQC for clarity. *indicates Trp side chain.

Extent of assignments and data deposition

Most of backbone resonances (90% of ^{15}N, 90% of H^N, 92% of C^α, 76% of H^α, 92% of C^β, and 79% of C′) and a part of aliphatic side-chain resonances have been assigned and deposited in the BioMagResBank (http://www.bmrb.wisc.edu) under an accession number of 6025.

Figure 1 shows the ^{1}H-^{15}N HSQC spectrum of ^{15}N/^{13}C-labeled $(His)_6$-LECT2. A six-residue segment ranging from 100 to 105 and six other residues at positions 19, 24, 25, 38, 51 and 143 remain unassigned as well as the N-terminal His_6-tag. The assignments of these residues have been hampered due to severe overlaps of NMR signals and possible fast exchanges of H^N involved.

The secondary structure prediction by CSI indicates that LECT2 contains several β-strands but no α-helix, which is consistent with the far-UV CD (circular dichroism) data (Ito et al., 2003).

Acknowledgements

This work was supported in part by Grants-in-Aid for Scientific Research and the National Project on Protein Structural and Functional Analyses from the Ministry of Education, Culture, Sports, Science and Technology of Japan.

References

Delaglio, F., Grzesiek, S., Vuister, G.W., Zhu, G., Pfeifer, J. and Bax, A. (1995) *J. Biomol. NMR*, **6**, 277–293.

Hiraki, Y., Inoue, H., Kondo, J., Kamizono, A., Yoshitake, Y., Shukunami, C. and Suzuki, F. (1996) *J. Biol. Chem.*, **271**, 22657–22662.

Ito, M., Nagata, K., Kato, Y. Oda, Y., Yamagoe, S., Suzuki, K. and Tanokura, M. (2003) *Protein Expr. Purif.*, **27**, 272–278.

Kameoka, Y., Yamagoe, S., Hatano, Y., Kasama, T. and Suzuki, K. (2000) *Arthritis Rheumatism*, **43**, 1419–1420.

Shukunami, C., Kondo, J., Wakai, H., Takahashi, K., Inoue, H., Kamizono, A. and Hiraki, Y. (1999) *J. Biochem.*, **125**, 436–442.

Wishart, D.S. and Sykes, B.D. (1994) *J. Biomol. NMR*, **4**, 171–180.

Wishart, D.S., Bigam, C.G., Yao, J., Abildaard, F., Dyson, H.J., Oldfield, E., Markley, J.L. and Sykes, B.D. (1995) *J. Biomol. NMR*, **6**, 135–140.

Yamagoe, S., Mizuno, S. and Suzuki, K. (1998a) *Biochim. Biophys. Acta*, **1396**, 105–113.

Yamagoe, S., Watanabe, T., Mizuno, S. and Suzuki, K. (1998b) *Gene*, **216**, 171–178.

Yamagoe, S., Yamakawa, Y., Matsuo, Y., Minowada, J., Mizuno, S. and Suzuki, K. (1996) *Immunol. Lett.*, **52**, 9–13.

Journal of Biomolecular NMR 30: 109–110, 2004.

Letter to the Editor: Backbone ^{1}H, ^{13}C and ^{15}N resonance assignment of the N-terminal domain of human eRF1

Yoshifumi Oda[a], Tomonari Muramatsu[b], Fumiaki Yumoto[a], Mie Ito[a] & Masaru Tanokura[a,*]
[a]*Department of Applied Biological Chemistry, Graduate School of Agricultural and Life Sciences, Bunkyo-ku, Tokyo 113-8657, Japan;* [b]*Cancer Medicine and Biophysics Division, National Cancer Center Research Institute, Chuo-ku, Tokyo 104-0045, Japan*

Received 24 March 2004; Accepted 29 April 2004

Key words: codon recognition, eRF1, human, NMR assignment, release factor, translation termination

Biological context

In translation termination processes, an in-frame stop codon (either UAG, UGA or UAA) is recognized directly by a class-I release factor (RF1/RF2 in prokaryotes and eRF1 in eukaryotes). The eukaryotic release factor eRF1 recognizes all three of those stop codons, but not the Trp codon UGG. This discrimination must require some conformational changes in the recognition domain of eRF1, because the UGG codon cannot be eliminated if eRF1 recognizes the stop codons by simply binding to A/G as the second letter and A/G as the third. Indeed, although human eRF1's crystal structure was reported (Song et al., 2000), the recognition mechanism has not been clearly illustrated. Muramatsu et al. published the hypothesis that the stop codon triplet is bound in the region containing the C-terminus of α2-helix of eRF1 (Glu55-Asn61) and that the discrimination of the three stop codons from the Trp codon requires a structure consisting of two α-helices (α2 and α3) and two β-strands (β1 and β4), which regulate the conformational flexibility of the tip region (Muramatsu et al., 2001). Recently, cross-linking experiments between eRF1 and mRNA in ribosome suggested that the entire domain is involved in the recognition (Chavatte et al., 2003). Thus, to address the mechanism underlying stop codon recognition, it is important to investigate the dynamic structure of this domain in solution. Here we report ^{1}H, ^{15}N and ^{13}C resonance assignments for the N-terminal domain [Met_1-Asp_{142}] of human eRF1.

*To whom correspondence should be addressed. E-mail: amtanok@mail.ecc.u-tokyo.ac.jp

Methods and experiments

The cDNA region coding for the N-terminal domain [Met_1-Asp_{142}] of human eRF1 was amplified by RT-PCR using human stomach total RNA (BD Biosciences Clontech, Palo Alto, CA) as a template and was then subcloned into pTWIN1 (New England Biolabs, Beverly, MA). This domain, accompanied by chitin-binding domains at both the N- and C-termini, was overproduced in *E. coli* Origami(DE3)pLacI (Novagen, Madison, WI). Then both of the chitin binding domains were removed by the affinity purification procedure described by the supplier (New England Biolabs), and the N-terminal domain of human eRF1 was further purified by cation exchange chromatography. The recombinant protein obtained by this protocol has additional N-terminal residues (Gly-Arg) and an additional C-terminal residue (Met). ^{15}N-labeled and $^{13}C/^{15}N$-labeled proteins were obtained by the same expression system described above in C.H.L. media (^{15}N: 95% and ^{15}N, ^{13}C: 95%, respectively) (Shoko, Tokyo). These purified proteins were dialyzed against NMR buffer (20 mM Na-phosphate (pH 6.0), 100 mM NaCl, 2 mM DTT and 0.02% NaN_3 in 90% H_2O/10% D_2O) and concentrated to approximately 0.5 mM with size-exclusion filters (Orbital Biosciences, Topsfield, MA).

All NMR data were recorded at 298K on Unity Inova 600 spectrometers (Varian Inc., Palo Alto, CA). HNCA, HN(CO)CA, HNCACB and CBCA(CO)NH spectra were used to attain assignments of backbone resonances. All data were processed using NMRPipe (Delaglio et al., 1995) and analyzed using Sparky (T.D. Goddard and D.G. Kneller, SPARKY 3, University of California, San Francisco). ^{1}H chemical shifts

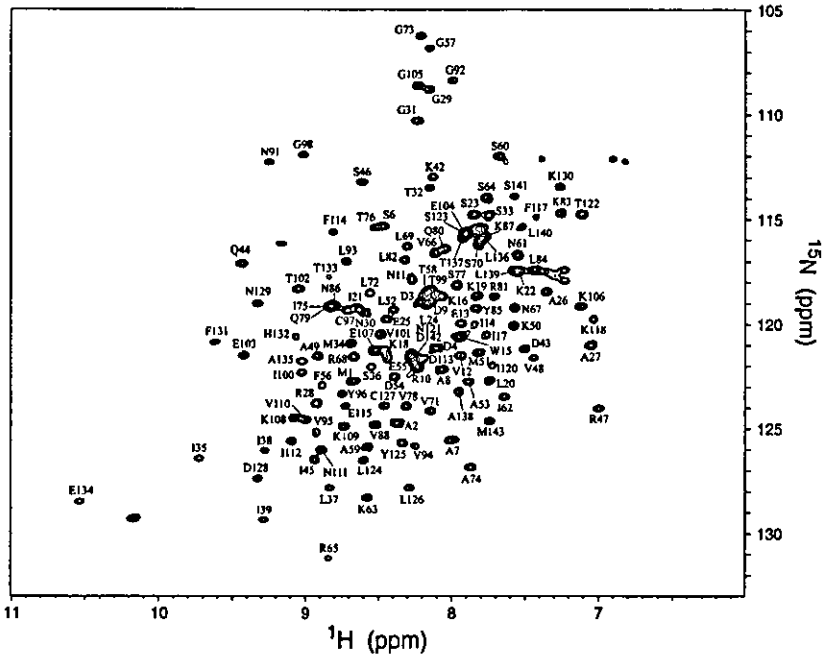

Figure 1. 2D ^{1}H-^{15}N HSQC spectrum with assignments of N-terminal domain of human eRF1 in 20 mM Na-phosphate (pH 6.0), 100 mM NaCl, 2 mM DTT and 0.02% NaN_3 in 90% H_2O/10% D_2O at 298K. The numbering of the residues follows the residue numbers of native eRF1 except for the non-native additional residue M143. Side chain peaks are not labeled.

were referenced to the ^{1}H resonance frequency of DSS (Wishart et al., 1995).

Extent of assignment and data deposition

Figure 1 shows the 2D ^{1}H-^{15}N HSQC spectrum of the N-terminal domain [Met_1-Asp_{142}] of human eRF1. All $^{1}H^{N}$ and ^{15}N resonances of native non-proline backbone residues have been assigned. Definitive assignments for the two N-terminal non-native residues have not been obtained due to the rapid amide proton exchange with water. The assigned ^{1}H, ^{13}C and ^{15}N chemical shifts have been deposited in the BioMagResBank database (http://www.bmrb.wisc.edu) under BMRB accession number 6116.

Acknowledgements

This work was supported in part by Grants-in-Aid for Scientific Research from the Ministry of Education, Science, Sports, and Culture of Japan and by a Grant-in-Aid for Research on Advanced Medical Technology from the Ministry of Health, Labour, and Welfare of Japan.

References

Chavatte, L., Kervestin, S., Favre, A. and Jean-Jean, O. (2003) *EMBO J.*, **22**, 1644–1653.

Delaglio, F., Grzesiek, S. Vuister, G.W., Zhu, G., Pfeifer, J. and Bax, A. (1995) *J. Biomol. NMR*, **6**, 277–293.

Muramatsu, T., Heckmann, K., Kitnaka, C. and Kuchino, Y. (2001) *FEBS Lett.*, **488**, 105–109.

Song, H., Mugnier, P., Das, A.K., Webb, H.M., Evans, D.R., Tuite, M.F., Hemmings, B.A. and Barford, D. (2000) *Cell*, **100**, 311–321.

Wishart, D.S., Bigam, C.G., Yao, J., Abildgaard, F., Dyson, H.J., Oldfield, E., Markley, J.L. and Sykes, B.D. (1995) *J. Biomol. NMR*, **6**, 135–140.

Biol. Chem., Vol. 385, pp. 381–388, May 2004

Identification of arginine residues important for the activity of *Escherichia coli* signal peptidase I

Yong-Tae Kim[1,a,b,*], Ryo Kurita[1,a], Masaki Kojima[2], Wataru Nishii[2], Masaru Tanokura[3], Tomonari Muramatsu[4], Hisashi Ito[1] and Kenji Takahashi[2]

[1]Department of Chemistry, Aoyama Gakuin University, Sagamihara, Kanagawa 229-8558, Japan
[2]School of Life Science, Tokyo University of Pharmacy and Life Science, Hachioji, Tokyo 192-0392, Japan
[3]Graduate School of Agricultural and Life Sciences, University of Tokyo, Bunkyo-ku, Tokyo 113-8657, Japan
[4]Biophysics Division, National Cancer Research Institute, Tokyo 104-0045, Japan

*Corresponding author
e-mail: yong-tae-kim@omrf.ouhsc.edu

Abstract

Escherichia coli signal peptidase I (leader peptidase, SPase I) is an integral membrane serine protease that catalyzes the cleavage of signal (leader) peptides from pre-forms of membrane or secretory proteins. We previously demonstrated that *E. coli* SPase I was significantly inactivated by reaction with phenylglyoxal with concomitant modification of three to four of the total 17 arginine residues in the enzyme. This result indicated that several arginine residues are important for the optimal activity of the enzyme. In the present study, we have constructed 17 mutants of the enzyme by site-directed mutagenesis to investigate the role of individual arginine residues in the enzyme. Mutation of Arg^{127}, Arg^{146}, Arg^{198}, Arg^{199}, Arg^{226}, Arg^{236}, Arg^{275}, Arg^{282}, and Arg^{295} scarcely affected the enzyme activity *in vivo* and *in vitro*. However, the enzymatic activity toward a synthetic substrate was significantly decreased by replacements of Arg^{77}, Arg^{222}, Arg^{315}, or Arg^{318} with alanine/lysine. The k_{cat} values of the R77A, R77K, R222A, R222K, R315A, R318A, and R318K mutant enzymes were about 5.5-fold smaller than that of the wild-type enzyme, whereas the K_m values of these mutant enzymes were almost identical with that of the wild-type. Moreover, the complementing abilities in *E. coli* IT41 were lost completely when Arg^{77}, Arg^{222}, Arg^{315}, or Arg^{318} was replaced with alanine/lysine. The circular dichroism spectra and other enzymatic properties of these mutants were comparable to those of the wild-type enzyme, indicating no global conformational changes. However, the thermostability of R222A, R222K, R315A, and R318K was significantly lower compared to the wild type. Therefore, Arg^{77}, Arg^{222}, Arg^{315}, and Arg^{318} are thought to be important for maintaining the proper and stable conformation of SPase I.

[a]These authors contributed equally to this work
[b]Present address: Oklahoma Medical Research Foundation, FRB&A, 825 NE 13th St., Oklahoma City, OK 73104, USA

Keywords: active site; arginine residue; leader peptidase; signal peptidase I; signal peptide; structure-function relationships.

Introduction

Most membrane and secretory proteins in *Escherichia coli* are synthesized *in vivo* as precursors that bear an amino-terminal signal (leader) peptide of 15 to 30 amino acid residues. This signal sequence is involved in guiding the protein into the targeting and translocating pathway by interacting with the membrane and other components of the cellular secretory machinery. The signal peptides are removed by the action of signal peptidase I (leader peptidase, SPase I) during or shortly after the protein export (Wolfe et al., 1983; Wickner et al., 1991; Paetzel et al., 2000). Following the discovery of *E. coli* SPase I by Chang and co-workers (1978), the gene encoding the enzyme was cloned (Date and Wickner, 1981), sequenced (Wolfe et al., 1983), overexpressed (Dalbey and Wickner, 1985; Kim et al., 1995a), purified (Zwizinski and Wickner, 1980; Wolfe et al., 1982; Kim et al., 1995a), and enzymatically characterized (Tschantz et al., 1993; Kim et al., 1995a) from a wild-type strain of *E. coli*. The substrate specificity of SPase I has also been investigated, which revealed that small uncharged amino acids are usually present at the -1 and -3 positions from the cleavage site (von Heijne, 1983). This enzyme is a typical Type I integral membrane endopeptidase anchored to the membrane by amino-terminal transmembrane segments (Moore and Miura, 1987; Bilgin et al., 1990). The active site and the substrate recognition site of the enzyme are in the carboxyl-terminal domain that resides on the outer surface of the cytoplasmic membrane (Zimmermann et al., 1982; Wolfe et al., 1983). Furthermore, a soluble catalytically active SPase I (Δ2–75 SPase I), which lacks the two amino-terminal transmembrane segments (residues 1–22 and residues 62–75) and the cytoplasmic domain (residues 23–61), has been produced (Kuo et al., 1993) and crystallized (Paetzel et al., 1998, 2002).

By using site-directed mutagenesis and chemical modification (Sung and Delbey, 1992; Black, 1993; Tschantz et al., 1993; Paetzel et al., 1997), it was shown that the catalytic activity of SPase I depends on the operation of a serine-lysine catalytic dyad, where Ser^{90} serves as the nucleophile and Lys^{145} serves as the general base in the catalytic mechanism. The serine-lysine catalytic dyad structure of SPase I has been recently confirmed by the three-dimensional structure of the enzyme in complex with a β-lactam inhibitor (Paetzel et al., 1998). Results of the enzymatic characterization, site-directed mutagenesis, chemical modification, and three-dimensional structure determination indicated that *E. coli* SPase I belongs to a novel class of serine protenases (Black

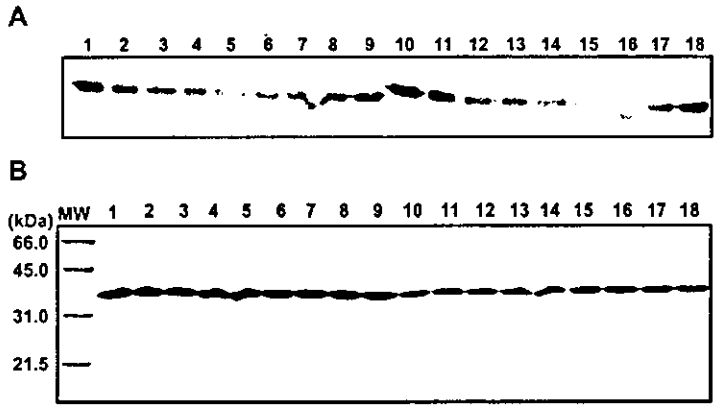

Figure 1 Western blot analysis and SDS-PAGE of the purified SPase I mutants.
(A) The lysates from *E. coli* MV1190 harboring the wild-type or mutant plasmids were separated by SDS/PAGE and subjected to Western blotting as described in the materials and methods section. (B) SDS/PAGE of the mutant enzymes was performed on a 12.5% polyacrylamide gel under reducing conditions followed by Coomassie Brilliant Blue staining. Lane 1, wild-type; lane 2, R77A; lane 3, R77K; lane 4, R127A; lane 5, R146A; lane 6, R198A; lane 7, R199A; lane 8, R222A; lane 9, R222K; lane 10, R226A; and lane 11, R236A; lane 12, R275A; lane 13, R282A; lane 14, R295A; lane 15, R315A; lane 16, R315K; lane 17, R318A; lane 18, R318K. M, molecular mass markers.

et al., 1992; Sung and Delbey, 1992; Black, 1993; Kuo et al., 1994; Kim et al., 1995a,b; Paetzel et al., 1997), which utilize a Ser-Lys catalytic dyad mechanism as opposed to the more common Ser-His-Asp catalytic triad mechanism in the cleavage reaction (Paetzel et al., 2000).

In order to shed light on the functional roles of amino acid residues of SPase I, we previously investigated the effects of various chemical modification reagents on the activity of the enzyme and found, by using phenylglyoxal, that the three or four arginine residues of the enzyme are important for the activity (Kim et al., 1995a). To further investigate the functional role of the arginine residues, in the present study we replaced the arginine residues with alanine and/or lysine by site-directed mutagenesis and examined the effects of the replacements on the enzymatic activities *in vitro* and *in vivo*. The results obtained strongly suggest that Arg^{77}, Arg^{222}, Arg^{315}, and Arg^{318} are important for the optimal activity of *E. coli* SPase I.

Results

Enzyme expression and purification

All arginine residues in *E. coli* SPase I were individually replaced with alanine and/or lysine by site-directed mutagenesis to obtain the following mutant enzymes: R77A, R77K, R127A, R146A, R198A, R199A, R222A, R222K, R226A, R236A, R275A, R282A, R295A, R315A, R315K R318A, and R318K. The mutant enzymes were constructed in the cloned *lep* gene and expressed in *E. coli* strain MV1190/pT7-7 under control of the T7 promoter. The induction conditions for the mutants of SPase I were investigated by means of Western blot analysis. Figure 1A shows that the protein expression efficiency of the mutants in *E. coli* MV1190 was similar to that of the wild-type enzyme. All the expressed mutants were purified by successive column chromatographic procedures using DAEA-cellulose, Mono P, and Sephadex G-75 as described previously (Kim et al., 1995a). All mutant enzymes were purified to homogeneity, giving a single band on SDS-PAGE corresponding to an apparent molecular mass of 37 kDa, identical with that of the wild-type enzyme (Figure 1B). In each case, the mutant enzyme was produced in the amount of 0.3 to 1.5 mg per 1 liter of LB broth (Table 1).

Enzymatic activity of the mutant enzymes

The enzymatic activities of the mutant enzymes were determined using a synthetic peptide (FSASALA/KI; Table 1). The R127A, R146A, R198A, R199A, R226A, R236A, R275A, R282A, R295A, and R315K mutant enzymes retained nearly full catalytic activity as compared with the wild-type enzyme. In contrast, when Arg^{77}, Arg^{222}, Arg^{315}, and Arg^{318} were replaced by alanine, the corresponding mutant proteins (R77A, R222A, R315A, and R318A) exhibited activities that were less than 18% of that of the wild-type enzyme. Furthermore, the replacement of Arg^{77}, Arg^{222}, and Arg^{318} with lysine also significantly affected the enzymatic activity. We also measured the activity of all mutant enzymes using the *in vivo* assay (Table 1): none of the replacements of Arg^{127}, Arg^{146}, Arg^{198}, Arg^{199}, Arg^{226}, Arg^{236}, Arg^{275}, Arg^{282}, and Arg^{295} with alanine affected the cell viability of the *E. coli* IT41 that had been transformed with the mutant plasmids. However, R77A, R77K, R222A, R222K, R315A, R318A, and R318K mutant enzymes apparently have lost the enzymatic activity completely.

Kinetic studies on the mutant enzymes

The kinetic parameters (k_{cat}, K_m and k_{cat}/K_m) of the wild-type and all mutant enzymes were determined by the *in vitro* assay using the synthetic substrate described above (Table 2). The k_{cat} and K_m values of the R127A, R146A, R198A, R199A, R226A, R236A, R275A, R282A, R295A, and R315K mutant enzymes were similar to those of the wild-type enzyme. However, the k_{cat} values of the R77A, R222A, R315A, and R318A mutant enzymes were reduced to less than 30% of that of the wild-type enzyme, while the K_m values of the mutants remained almost unchanged. The replacements with lysine of

Table 1 Enzymatic activities of the wild-type SPase I and its mutants.

Enzyme	Relative enzyme amount produced	*In vitro* assay		*In vivo* assay Cell viability
		Specific activity (Units/mg)	Relative activity (%)	
Wild-type	1.00	12 800±130	100±1	yes
R77A	0.81	1660±100	13±1	no
R77K	0.20	5568±250	43±2	no
R127A	0.18	11 650±520	91±4	yes
R146A	0.26	12 630±120	99±1	yes
R198A	0.67	11 120±110	87±1	yes
R199A	1.03	13 700±230	107±2	yes
R222A	1.04	1700±100	13±1	no
R222K	0.88	3145±100	25±1	no
R226A	0.45	10 770±250	84±2	yes
R236A	0.61	13 600±100	106±1	yes
R275A	0.60	12 900±320	101±3	yes
R282A	0.90	11 900±250	93±2	yes
R295A	0.85	12 880±120	101±1	yes
R315A	0.80	2320±100	18±1	no
R315K	1.21	9088±250	71±2	yes
R318A	0.19	1040±110	8±1	no
R318K	1.10	390±100	3±2	no

The activities were determined by measuring the initial rates of the substrate hydrolysis. One U is defined as the activity hydrolyzing 1 pmol of synthetic peptide/min. The relative activity in the *in vivo* assay was estimated from the increase in absorbance at 600 nm of *E. coli* IT41/pGP1-2 encoding mutant leader peptidases relative to that encoding the wild-type enzyme. Values are mean±SD, generally based on at least five independent determinations ($n \geq 5$).

Arg^{77}, Arg^{222}, and Arg^{318} significantly affected the k_{cat} value, but that of Arg^{315} did not significantly affect the k_{cat} value.

Structural comparison and thermostability of the mutant enzymes

Far-UV circular dichroism (CD) spectra were recorded to compare the secondary structures of the R77A, R222A, R315A, and R318A mutant enzymes with that of the wild-type SPase I. As shown in Figure 2, the CD spectra of the mutant enzymes as well as those of other mutant enzymes (data not shown) were nearly identical with that of the wild-type enzyme. These results indicated that no gross misfolding or changes in the secondary structure of the enzymes were induced by introduction of the mutations. We predicted the three-dimensional structure of the mutants R77A, R222A, R315A, and R318A by computer modeling using the wild-type atomic coordinates as the initial structure. However, the results indicated that all mutants had almost the same conformation as the wild-type enzyme (data not shown), consistent with the results of the CD measurements.

Figure 3 shows the thermostability profiles of the proteins carrying replacements of Arg^{77}, Arg^{222}, Arg^{315}, and Arg^{318} with alanine and lysine, respectively. After incubation of the enzymes at pH 7.0 and various temperatures for 60 min, the remaining activities were assayed. The R77A, R77K, R315K, and R318A mutant enzymes as well as the wild-type enzyme were fairly stable at temperatures up to 40°C, but were inactivated progressively above 40°C. When the enzymes were incubated at 48°C, the wild-type enzyme was inactivated to an extent of about 95%, whereas R77A, R77K, R315K, and R318A were inactivated to 70–95%. The wild-type and mutant enzymes were completely inactivated by incubation at 50°C. Thus, the temperature/stability profiles are roughly similar between the wild-type and these mutant enzymes. However, R222A and R222K were only stable at temperatures up to 30°C. The R222A and R222K mutant enzymes were completely inactivated at 42°C. The R315A and R318K mutants were also less stable than the wild-type enzyme.

Discussion

Our previous study using chemical modification demonstrated that several arginine resiudes are important for the enzymatic activity of *E. coli* SPase I. When at least three out of the 17 arginine residues in SPase I were modified by reaction with phenylglyoxal, nearly 70% of the activity was lost (Kim et al., 1995a). However, it was not clear whether these arginine residues in SPase I are important for the catalytic mechanism or the maintenance of the proper protein conformation. In the present study, we have used site-directed mutagenesis to investigate the role of each arginine residue in the catalytic domain (residue 76–323) of SPase I in more detail by substituting each arginine residue with alanine and/or lysine. The activities of R77A, R77K, R222A, R222K, R315A, R318A and R318K mutant enzymes were shown to be considerably lower than that of the wild-type enzyme as measured by both *in vitro* and *in vivo* assays. However, the enzymatic activities of the other mutant enzymes (R127A, R146A, R198A, R199A, R226A, R236A, R275A, R282A, R295A, and R315K) remained similar to that of the wild-type enzyme. These results are consistent with previous data obtained by chemical mod-

Table 2 Kinetic parameters for the wild-type SPase I and its mutants.

Enzyme	k_{cat} (h^{-1})	K_m (mM)	k_{cat}/K_m (h^{-1} mM^{-1})
Wild type	86.4	0.52	166.2
R77A	14.9	0.67	22.2
R77K	42.8	0.63	67.9
R127A	66.4	0.49	135.5
R146A	86.4	0.52	166.2
R198A	66.4	0.52	127.7
R199A	78.5	0.55	142.7
R222A	16.3	0.54	30.2
R222K	19.0	0.53	35.8
R226A	57.6	0.52	110.8
R236A	78.5	0.52	163.5
R275A	78.5	0.49	160.2
R282A	72.0	0.49	146.9
R295A	72.0	0.52	138.5
R315A	25.4	0.57	44.6
R315K	61.2	0.49	124.9
R318A	4.8	0.43	11.2
R318K	2.2	0.53	4.2

The initial rates were determined at 37°C in 25 mM sodium phosphate, pH 7.7. The concentration of the synthetic peptide (FSASALA/KI) was varied in the range of 0.04–0.8 mM. The kinetic data were analyzed by double-reciprocal plots. Values are mean±SD, generally based on $n \geq 3$.

ification with phenyglyoxal, which demonstrated that several arginine residues in SPase I are important for the enzymatic activity (Kim et al., 1995a). The results with R146A and R282M are consistent and somewhat inconsistent, respectively, with those obtained previously (Klenotic et al., 2000). The discrepancies may be partly due to the difference in the assay method used. In the assay using a synthetic peptide (FSASALA/KI) as substrate, the k_{cat} values of R77A, R222A, R315A, and R318A were shown to be less than 18% of that of the wild-type enzyme but they still retained some activity, whereas the K_m values were similar to that of the wild-type enzyme (Table 2). Therefore, the Arg^{77}, Arg^{222}, Arg^{315}, and Arg^{318} residues appear to be somehow important for the activity, but not to be directly involved in catalysis or binding of the substrate to the enzyme. On the other hand, in the *in vivo* assay, the R77A, R77K, R222A, R222K, R315A, R318A, and R318K mutants were shown to have apparently no activity. Thus, the activities determined by both assays are somewhat different. This may be due to the difference in the activity of SPase I toward the synthetic peptide substrate used in the *in vitro* assay and toward the natural substrates *in vivo* that are thought to be the real targets of SPase I in the *in vitro* assay. It may also be possible that a nonviable phenotype of these mutants is a simple result of insufficient catalytic activity of mutated SPase I. Indeed, from the data in Table 1, it is apparent that mutants with a relative activity below 50% of the wild-type enzyme are nonviable and this corresponds to a catalytic efficiency (i.e., k_{cat}/K_m) below 100 (Table 2).

The alignment of the amino acid sequences of the SPases I of *E. coli*, *S. typhimurium*, *B. subtilis* (SipS), and *S. cerevisiae* (Imp1P) revealed five regions of similarity denoted as follow: boxes A (residues 72–76, membrane-anchor domain), B (residues 88–96), C (residues 127–133), D (residues 137–154), and E (residues 272–282) (van Dijl et al., 1992; Dalbey et al., 1997). The recent determination of the crystal structure of the catalytic domain of *E. coli* SPase I indicated that most of the amino acids that are strictly conserved in boxes B, C, D, and E of the type I SPase family are found near the active site (Paetzel et al., 1998, 2000). The catalytic site Ser^{90} (nucleophile) and Lys^{145} (general base) of the SPase family are conserved in box B and box D, respectively. On the other hand, Arg^{127} (in box B), Arg^{146} (in box D), Arg^{275} (in box E), and Arg^{282} (in box E) in SPase I are also conserved in prokaryotic and/or eukaryotic Type 1 SPase families. In addition, the crystal structure has revealed that Arg^{146} and Arg^{282} form salt bridges with Asp^{273} and Asp^{280}, respectively (Paetzel et al., 1998, 2000). However, the SPase I mutant enzymes R127A, R146A, R275A, and

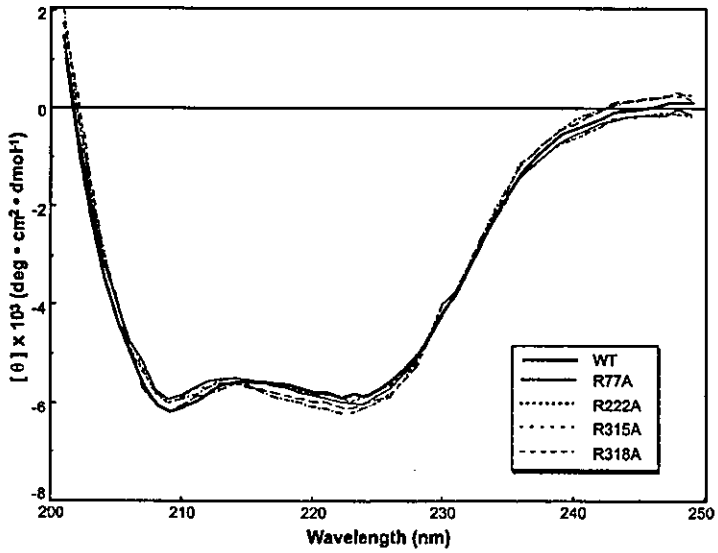

Figure 2 Far-ultraviolet CD spectra of the wild-type SPase I and its mutants.
The CD spectra were measured using a 0.1 cm cuvette at 25°C and at a protein concentration of 2.0 μM in 25 mM sodium phosphate buffer, pH 7.7, containing 0.1% Lubrol PX and 10% glycerol. For the other conditions see the materials and methods section.

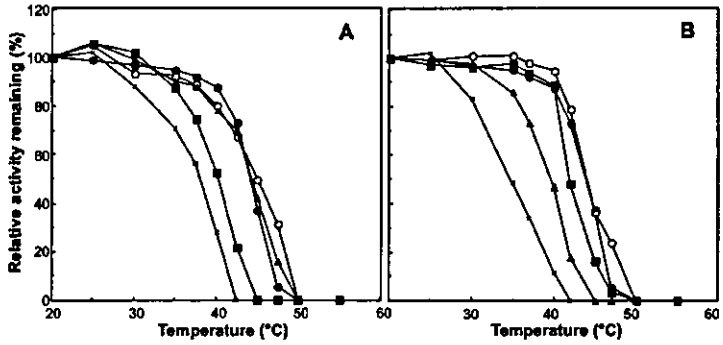

Figure 3 Thermostability of the wild-type SPase I and its mutants.
The enzyme was incubated at each temperature for 1 h in 10 mM potassium phosphate, pH 7.0, containing 0.1% Lubrol PX, 10% glycerol and 35 mM NaCl, and the remaining activity was determined using the peptide substrate as described in the materials and methods section. (A) Wild-type (solid circle); R77A (open circle); R222A (cross); R315A (solid square); R318A (solid triangle). (B) Wild-type (solid circle); R77K (open circle); R222K (cross); R315K (solid square); R318K (solid triangle).

R282A, all maintained nearly the same activity as the wild-type enzyme, indicating that these residues are not critical for the catalytic activity of SPase I, and hence that the salt bridges of Arg^{146}-Asp^{273} and Arg^{282}-Asp^{280} are not important for the activity.

In contrast, Arg^{77}, Arg^{222}, Arg^{315}, and Arg^{318} in SPase I are necessary for efficient enzymatic catalysis, as demonstrated by the *in vivo* and *in vitro* assays. Deletion studies on *E. coli* SPase I showed that the C-terminal hydrophilic domain (residue 77–323) exposed to the periplasm constitutes the catalytic domain (Bilgin et al., 1990). It was also suggested that Arg^{77} of SPase I might be important for catalysis (Bilgin et al., 1990), which is consistent with our data indicating that Arg^{77} is critical for the enzyme activity. The specific activities of the R77A and R77K mutant enzymes were significantly decreased in spite of little change in enzymatic properties, secondary structure, and predicted conformation of the mutants compared with those of the wild-type enzyme. Although Arg^{77} is located far from the active site of SPase I in the three-dimensional structure (Paetzel et al., 2000), it interacts with Tyr^{108} and Ile^{110} which are directly connected to the active site residue Ser^{90} (Figure 4). The mutation of Arg^{77} may cause a slight shift of the position of this segment (Ser^{90}-Tyr^{108}-Ile^{110}), leading to the oberseved loss of activity.

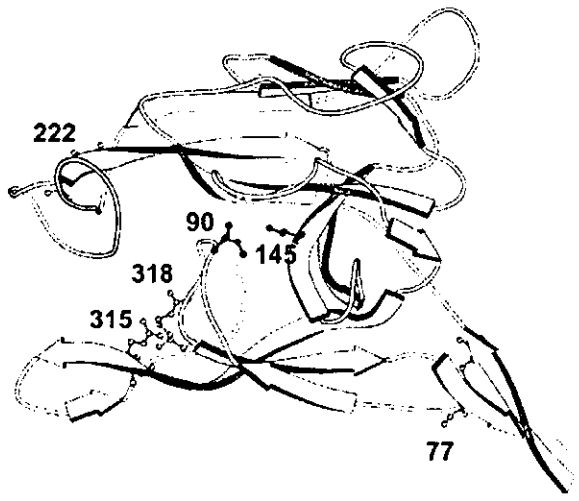

Figure 4 Schematic representation of the backbone conformation of SPase I.
The side chains of Ser^{90} and Lys^{145} (black) and Arg^{77}, Arg^{222}, Arg^{315}, and Arg^{318} (grey) are drawn in a ball-and-stick model with residue numbers indicated. The structure was prepared from the PDB atomic coordinates 1B12 (Paetzel et al., 1998) with a slight modification using the program MolScript (Kraulis, 1991).

On the other hand, when Arg^{222} that is located near the β-sheet domain II in the *E. coli* SPase I (Paetzel et al., 1998) was substituted with alanine/lysine, the catalytic activity was drastically lost *in vitro* and *in vivo*. In the assay using the synthetic peptides as substrate, the k_{cat} values of R222A and R222K were about 20% of that of the wild-type enzyme, whereas the K_m values were similar to that of wild-type SPase I (Table 2). The mutant enzymes behaved like the wild-type enzyme throughout the expression and purification steps, and their isoelectric points and secondary structures were essentially the same as that of the wild-type enzyme. In the three-dimensional structure, Arg^{222} was suggested to interact with the side chains of Thr^{216} and Pro^{212} and the carbonyl groups in the main chain of Asp^{191} and Glu^{215} (Figure 4). Although the mutation of Arg^{222} may cause a local conformational change of these and neighboring residues, details are unclear from the three-dimensional structure and the CD spectra. On the other hand, the thermostability of the R222A and R222K mutant enzymes were markedly lower than that of the wild-type SPase I, indicating that Arg^{222} is important for protein stability.

We also found that Arg^{315} and Arg^{318}, located at the small 3_{10}-helix domain (residues 315–319) of the C-terminus of *E. coli* SPase I (Paetzel et al., 1998), are important for the catalytic activity. The replacements of Arg^{315} and Arg^{318} with alanine markedly decreased the specific activities both *in vivo* and *in vitro*. The k_{cat} values of the R315A and R318A mutant enzymes were 29% and 5%, respectively, of that of wild-type enzyme, whereas the K_m values were similar to that of the wild-type SPase I (Table 2). Other enzymatic properties (data not shown) and the CD spectra of the R315A and R318A mutant enzymes were similar to those of the wild-type enzyme. The thermostability of R318A was also similar to that of the wild-type enzyme although R315A had somewhat decreased thermostability. These results show that, except for changes in activity, the mutations did not result in marked

changes in general properties of the enzyme including its conformation. In the three-dimensional structure, Arg^{315} interacts with Asp^{99} and Ile^{97}, and Arg^{318} interacts with Leu^{96} (Figure 4). These interacting residues are located near the catalytic residue Ser^{90}. The mutation of Arg^{315} or Arg^{318} to Ala may change the orientation of Ser^{90} through interaction with the neighboring residues. The R315K mutant retained high activity; this indicates that Arg^{315} may be replaced with a positively changed Lys residue without much loss of activity.

From these results, we conclude that Arg^{77}, Arg^{222}, Arg^{315}, and Arg^{318} play an important role in the enzymatic activity of *E. coli* SPase I, although they may not be directly involved in catalysis. It seems most likely that these residues are somehow involved in maintenance of the proper, enzymatically active and stable conformation and/or favorable microenvironment of the active site that is important for catalysis. However, its implication in substrate binding cannot be completely excluded. Further studies are necessary to elucidate the precise role of these residues.

Materials and methods

Bacterial strains, plasmids, and materials

E. coli strain MV1190 was used as a host for the expression vector pT7-7 as well as for the overproduction of the wild-type and mutant proteins. The pT7-7 plasmid that has the T7 promoter and the M13 phage mGP1-2 and pGP1-2 plasmids carrying the T7 polymerase gene were obtained from Dr. S. Tabor (Tabor, 1990). The plasmid pT7-7/*lep* was used for overproduction of SPase I in *E. coli* MV1190 as described previously (Kim et al., 1995a). *E. coli* strain IT41 encoding a chromosomal temperature-sensitive SPase I was a gift from Dr. Y. Nakamura (Inada et al., 1989). Restriction endonucleases, DNA amplification reagents, and *Taq* DNA polymerase were purchased from Toyobo (Tokyo, Japan) and the T4 DNA ligation kit was obtained from Takara (Kyoto, Japan). The reagents for DNA sequencing were from Applied Biosystem (Foster City, USA). All other reagents used were of analytical grade and obtained from Wako Pure Chemicals (Osaka, Japan).

Site-directed mutagenesis and enzyme expression

The DNA manipulations were carried out as described by Sambrook et al. (1989). Site-directed mutagenesis was performed according to the procedure of Kunkel (1985). The oligonucleotide primers used for this mutagenesis are listed in Table 3. The mutations were confirmed by DNA sequencing. Each of the mutated genes was inserted back into the corresponding portion of the pT7-7/*lep* expression vector (Kim et al., 1995a). The mutant enzymes were expressed and purified as described previously (Kim et al., 1995a,b).

In vitro and *in vivo* SPase I activity assay

To determine the enzymatic activity of the mutant enzymes *in vitro*, we used the chemically synthesized peptide substrate (FSASALAKI) corresponding to part of the maltose-binding protein precursor containing the cleavage site (A/K) of SPase I. In the routine assay, a 10 µl aliquot of each enzyme was added to 40 µl of substrate at a final concentration of 0.4 mM in 25 mM sodium phosphate, pH 7.7. The reaction was allowed to proceed at 37°C for 30 min, and stopped by the addition of 50 µl of 0.1% trifluoroacetic acid, and the reaction mixture was subsequenly analyzed by HPLC using a C_{18} column as described previously (Kim et al., 1995a). The activity of SPase I *in vivo* was determined using the temperature-sensitive *E. coli* SPase I strain IT41 (Inada et al., 1989). Measurement of SPase I activity *in vivo* was performed as described previously (Kim et al., 1995b).

Kinetic studies

Kinetic parameters (k_{cat}, K_m, and k_{cat}/K_m) for the synthetic substrate (FSASALA/KI) were determined as described previously (Kim et al., 1995b). The reaction was initiated by the addition of each mutant enzyme to a substrate solution containing 25 mM sodium phosphate, pH 7.7. The reactions were carried out at 37°C at six or more different initial substrate concentrations (0.04–0.8 mM). The enzyme concentration used in kinetic experiments was 1.69 µM.

Determination of thermostability

To test the thermostability, the wild-type and mutant enzymes in 10 mM potassium phosphate, pH 7.0, containing 0.1% Lubrol PX, 10% glycerol and 35 mM NaCl were incubated at the indi-

Table 3 Oligonucleotide primers used to construct SPase I mutations.

Primer	Sequence	Direction
R77A	5'-TATTGATTGTGGCTTCGTTTATTT-3'	forward
R77K	5'-TATTGATTGTGAAATCGTTTATTT-3'	forward
R127A	5'-GTCATCCGAAAGCCGGCGATATCG-3'	forward
R146A	5'-ATTACATCAAGGCCGCGGTGGGTT-3'	forward
R198A	5'-CACCATTACGGGCTGAGAAGGTCT-3'	reverse
R199A	5'-CCCCACCATTAGCGCGTGAGAAGG-3'	reverse
R222A	5'-GCTCGGAAAGAGCAATTCCATTTTC-3'	reverse
R222K	5'-GCTCGGAAAGTTTAATTCCATTTTC-3'	reverse
R226A	5'-GTGTCTCTTTAGCCTCGGAAAGAC-3'	reverse
R236A	5'-CTGTCAGAATGGCGTGCGTCACAT-3'	reverse
R275A	5'-CGCTGTTGTCCGCGTTGTCGCCCA-3'	reverse
R282A	5'-AGCCCCAGTAAGCGCTGTCCGCGC-3'	reverse
R295A	5'-TAGCCGTTGCCGCACCGACCAGAT-3'	reverse
R315A	5'-TGCGACTTAAGGCCAGACCAGTCG-3'	reverse
R315K	5'-TGCGACTTAATTTCAGACCAGTCG-3'	reverse
R318A	5'-TGCCGCCAATGGCACTTAAGCGCA-3'	reverse
R318K	5'-TGCCGCCAATTTTACTTAAGCGCA-3'	reverse

The codons that were changed by mutation are underlined.

cated temperatures for 1 h. Remaining activities were measured by mixing 10 μl of each heat-treated enzyme with 40 μl of the synthetic substrate solution. The reaction was allowed to proceed at 37°C for 30 min and was stopped by the addition of 50 μl of 0.1% trifluoroacetic acid. Then the reaction mixture was analyzed by HPLC as described previously (Kim et al., 1995a).

Circular dichroism spectroscopy

The circular dichroism (CD) spectra of the wild-type enzyme and its mutants were recorded at a protein concentration of 2.0 μM in 25 mM sodium phosphate buffer, pH 7.7, containing 0.1% Lubrol PX and 10% glycerol with a Jasco J-720 spectropolarimeter at room temperature using the water-jacketed quartz cell with a light path of 1 mm. The sample solutions were prepared by appropriately diluting the solutions of the enzyme with 25 mM sodium phosphate buffer, pH 7.7, just before measurement. For all measurements, a 1.0 nm band width and a 1.0 s time constant were used, and 32 scans were repeated from 200 to 250 nm at the speed of 50 nm/min with 0.1 nm/point resolution. The protein concentrations of the mutants used for CD spectroscopy were determined by amino acid analysis after acid hydrolysis

Western blot analysis

MV1190/pT7-7/*lep* and the mutants were grown in LB media to an absorbance at 600 nm of 0.7, and then the expression was induced with M13 phage mGP1-2 and IPTG (final concentration of 1 mM). After an additional 4 h incubation at 37°C, cell cultures (100 μl) were adjusted to a constant concentration by dilution and were pelleted; the pellets were resuspended in 2 volumes of the sample buffer. Aliquots (10 μl) of dissolved cell extracts were then subjected to 12.5% SDS-PAGE and the proteins were electroblotted onto polyvinylidene difluoride membranes (Bio-Rad; Hercules, USA). The immunoblots were blocked with phosphate-buffered saline (PBS) containing 1% bovine serum albumin (BSA) for 1 h at room temperature. The blocked membrane was probed with SPase I antiserum (20 μg/ml) in PBS buffer containing 1% BSA and 0.05% Tween 20. The membrane was washed and probed with alkaline phosphatase-conjugated goat anti-rabbit IgG (Pierce; Rockford, USA) as a secondary antibody (0.1 μg/ml) in 10 mM Tris-HCl (pH 8.0) containing 0.05% Tween 20. The antibody bound to the blots was visualized by the reaction with BCIP/NBT membrane phosphatase substrate (Pierce).

Acknowledgments

The authors thank Dr. S. Tabor, Harvard Medical School, for the kind gift of pT7-7 plasmid, M13 phage mGP1-2 and pGP1-2 plasmid; Dr. Y. Nakamura, Institute of Medical Science, The University of Tokyo, for providing us with *E. coli* IT41; Dr. S. Yokoyama, Department of Biophysics and Biochemistry, The University of Tokyo, for advice on CD experiments. This work was supported in part by Grants-in-Aid from the Ministry of Education, Science, Sports and Culture of Japan.

References

Bilgin, N., Lee, J. I., Zhu, H., Dalbey, R. and von Heijne, G. (1990). Mapping of catalytically important domains in *Escherichia coli* leader peptidase. EMBO J. *9*, 2717–2722.

Black, M. T., Munn, J. G. R. and Allsop, A. E. (1992). On the catalytic mechanism of prokaryotic leader peptidase I. Biochem. J. *282*, 539–543.

Black, M. T. (1993). Evidence that the catalytic activity of prokaryote leader peptidase depends upon the operation of a serine-lysine catalytic dyad. J. Bacteriol. *175*, 4957–4961.

Chang, C. N., Blobel, G. and Model, P. (1978). Detection of prokaryotic signal peptidase in an *Escherichia coli* membrane fraction: endoproteolytic cleavage of nascent f1 pre-coat protein. Proc. Natl. Acad. Sci. USA *75*, 361–365.

Dalbey, R. E. and Wickner, W. (1985). Leader peptidase catalyzes the release of exported proteins from the outer surface of the *Escherichia coli* plasma membrane. J. Biol. Chem. *260*, 15925–15931.

Dalbey, R. E., Lively, M. O., Bron, S. and van Dijl, J. M. (1997). The chemistry and enzymology of the type I signal peptidases. Protein Sci. *6*, 1129–1138.

Date, T. and Wickner, W. (1981). Isolation of the *Escherichia coli* leader peptidase gene and effects of leader peptidase overproduction *in vivo*. Proc. Natl. Acad. Sci. USA *78*, 6106–6110.

Inada, T., Court, D. L., Ito, K. and Nakamura, Y. (1989). Conditionally lethal amber mutations in the leader peptidase gene of *Escherichia coli*. J. Bacteriol. *171*, 585–587

Kim, Y.-T., Muramatsu, T. and Takahashi, K. (1995a). Leader peptidase from *Escherichia coli*: overexpression, characterization, and inactivation by modification of tryptophan residues 300 and 310 with *N*-bromosuccinimide. J. Biochem. (Tokyo) *117*, 535–544.

Kim, Y.-T., Muramatsu, T. and Takahashi, K. (1995b). Identification of Trp300 as an important residue for *Escherichia coli* leader peptidase activity. Eur. J. Biochem. *234*, 358–362.

Klenotic, P. A., Carlos, J. L., Samuelson, J. C., Schuenemann, T. A., Tschantz, W. R., Paetzel, M., Strynadka, N. C. J., and Dalbey, R. E. (2000). The role of the conserved Box E residues in the active site of the *Escherichia coli* Type I signal peptidase. J. Biol. Chem. *275*, 6490–6498.

Kraulis, P. J. (1991). MOLSCRIPT: a program to produce both detailed and schematic plots of protein structures. J. Appl. Cryst. *24*, 946–950.

Kunkel, T. A. (1985). Rapid and efficient site-specific mutagenesis without phenotypic selection. Proc. Natl. Acad. Sci. USA *82*, 488–492.

Kuo, D. W., Chan, H. K.,Wilson, C. J., Griffin, P. R., Williams, H. and Knight, W. B. (1993). *Escherichia coli* leader peptidase: production of an active form lacking a requirement for detergent and development of peptide substrates. Arch. Biochem. Biophys. *303*, 274–280.

Kuo, D., Weidner, J., Griffin, P., Shah, S. K. and Knight, W. B. (1994). Determination of the kinetic parameters of *Escherichia coli* leader peptidase activity using a continuous assay: the pH dependence and time-dependent inhibition by β-lactams are consistent with a novel serine protease mechanism. Biochemistry *33*, 8347–8354.

Moore, K. E. and Miura, S. (1987). A small hydrophobic domain anchors leader peptidase to the cytoplasmic membrane of *Escherichia coli*. J. Biol. Chem. *262*, 8806–8813.

Paetzel, M., Strynadka, N. C., Tschantz, W. R., Casareno, R., Bullinger, P. R. and Dalbey, R. E. (1997). Use of site-directed chemical modification to study an essential lysine in *Escherichia coli* leader peptidase. J. Biol. Chem. *272*, 9994–10003.

Paetzel, M., Dalbey, R. E. and Strynadka, N. C. J. (1998). Crystal structure of a bacterial signal peptidase in complex with a β-lactam inhibitor. Nature *396*, 186–190.

Paetzel, M., Dalbey, R. E. and Strynadka, N. C. J. (2000). The structure and mechanism of bacterial type I signal peptidases. A novel antibiotic target. Pharmacol. Ther. *87*, 27–49.

Paetzel, M., Dalbey, R. E. and Strynadka, N. C. J. (2002). Crystal structure of a bacterial signal peptidase apoenzyme: implications for signal peptide binding and the Ser-Lys dyad mechanism. J. Biol. Chem. *277*, 9512–9519.

Sambrook, J., Fritsch, E. F. and Maniatis, T. (1989). Molecular Cloning: A Laboratory Manual, 2nd Edition (Cold Spring Harbor, USA: Cold Spring Harbor Laboratory).

Sung, M. and Delbey, R. E. (1992). Identification of potential active-site residues in the *Escherichia coli* leader peptidase. J. Biol. Chem. *267*, 13154–13159.

Tabor, S. (1990). Expression using the T7 RNA polymerase/promoter system. In: Current Protocols in Molecular Biology, F. M. Ausubel, R. Brent, R. E. Kingston, D. D. Moore, J. G. Seidman, J. A. Smith and K. Struhl, eds. (New York, USA: Greene Publishing and Wiley Interscience), pp. 16. 2. 1–16. 2. 11.

Tschantz, W. R., Sung, M., Delgodo-Partin, V. M. and Delbey, R. E. (1993). A serine and a lysine residue implicated in the catalytic mechanism of the *Escherichia coli* leader peptidase. J. Biol. Chem. *268*, 27349–27354.

van Dijl, J. M., de Jong, A., Vehmaanperä, J., Venema, G. and Bron, S. (1992). Signal peptidase I of *Bacillus Subtilis*: patterns of conserved amino acids in prokaryotic and eukaryotic type I signal peptidase. EMBO J. *11*, 2819–2828.

von Heijne, G. (1983). Patterns of amino acids near signal-sequence cleavage sites. Eur. J. Biochem. *133*, 17–21.

Wickner, W., Driessen, A. J. M. and Hartl, F.-U. (1991). The Enzymology of protein translocation across the *Escherichia coli* plasma membrane. Annu. Rev. Biochem. *60*, 101–124.

Wolfe, P. B., Silver, P. and Wickner, W. (1982). The isolation of homogeneous leader peptidase from a strain of *Escherichia coli* which overproduces the enzyme. J. Biol. Chem. *257*, 7898–7902.

Wolfe, P. B., Wickner, W. and Goodman, J. M. (1983). Sequence of the leader peptidase gene of *Escherichia coli* and the orientation of leader peptidase in the bacterial envelope. J. Biol. Chem. *258*, 12073–12080.

Zimmermann, R., Watts, C. and Wickner, W. (1982). The biosynthesis of membrane-bound M13 coat protein. J. Biol. Chem. *257*, 6529–6536.

Zwizinski, C. and Wickner, W. (1980). Purification and characterization of leader (signal) peptidase from *Escherichia coli*. J. Biol. Chem. *255*, 7973–7977.

Received November 13, 2003; accepted February 20, 2004

P-29

ANALYSIS OF DYNAMIC STRUCTURE OF EUKARYOTIC RELEASE FACTOR 1 (eRF1)

Tomonari Muramatsu[1], Yoshifumi Oda[2], Fumiaki Yumoto[2], Mie Ito[2], Masaru Tanokura[2]
[1]Cancer Medicine & Biophysics Division, National Cancer Center Research Institute, Tokyo 104-0045, and [2]Department of Applied Biological Chemistry, Graduate School of Agricultural and Life Sciences, The University of Tokyo, 1-1-1 Yayoi, Bunkyo-ku, Tokyo 113-8657, Japan

In the translational step of genetic information, stop signals are recognizes not by tRNAs but by proteins called release factors (RFs). In prokaryotes, there are two RF species having distinct codon specificities: RF1 recognizes UAA and UAG, while RF2 recognizes UAA and UGA. In contrast, the single factor eRF1 in eukaryotes recognizes all of the three stop codons (UAA, UAG, and UGA). In this case some residues in eRF1 probably recognize A or G in the second position of a stop codon and other residues A or G in the third position. However, the two processes of recognition should not be achieved independently of each other given the fact that the tryptophan codon UGG is not recognized as a stop codon. This raises a question regarding the mechanism by which UGG is discriminated.

We have proposed a mechanism, where the amino acid residues 57/58 of eRF1 interact with the second and the residues 60/61 with the third position of a stop codon [1]. The fact that eRF1 recognizes all the three stop codons but not the codon for tryptophan (UGG) could be explained by the flexibility of the helix containing these residues. To test this hypothesis, we need to examine first whether the helix is flexible or not. We therefore prepared ^{15}N-labeled and ^{15}N/^{13}C-labeled 'codon recognition domains' containing the helix, and now are analyzing dynamic structure of this domain by NMR spectroscopy.

[1] T. Muramatsu *et al.*, *FEBS Lett.* **488**, 105-109 (2001)

The three-dimensional structure of aspergilloglutamic peptidase from *Aspergillus niger*

By Hiroshi SASAKI,[*1,*2] Atsushi NAKAGAWA,[*3] Tomonari MURAMATSU,[*4] Megumi SUGANUMA,[*5] Yoriko SAWANO,[*5] Masaki KOJIMA,[*6] Keiko KUBOTA,[*6] Kenji TAKAHASHI,[*1,*6] and Masaru TANOKURA[*1,*5,†]

(Communicated by Masanori OTSUKA, M. J. A.)

Abstract: Aspergilloglutamic peptidase from *Aspergillus niger* is a novel pepstatin-insensitive acid endopeptidase distinct from the well-studied aspartic peptidases, and thus is an interesting target for protein structure/function studies. In the present study, we have determined the three-dimensional structure of the enzyme by X-ray crystallography to a 1.4-Å resolution. The results revealed that the enzyme has a unique structure, composed of two seven-stranded anti-parallel β-sheets which form a β-sandwich structure and appear to have a partial two-fold symmetry, suggesting its possible evolution by gene duplication and that the glutamic acid-110 and glutamine-24 in the heavy chain form a catalytic dyad, consistent with our results obtained by site-directed mutagenesis.

Key words: Aspergilloglutamic peptidase; catalytic residue; glutamic peptidase; three-dimensional structure; X-ray crystallography.

Introduction. Aspergilloglutamic peptidase (AGP; *MEROPS* ID: G01.002; formerly called aspergillopepsin II) is an acid endopeptidase produced by the fungus *Aspergillus niger* var. *macrosporus*,[1,2] belonging to the newly established family of glutamic peptidases (i.e., peptidase family G1). AGP is unique among several homologous peptidases in that it is the only two-chain structure enzyme among them.[3] Moreover, it is completely different in amino acid sequence from the well-studied aspartic peptidases and is insensitive to aspartic peptidase-specific inhibitors, such as pepstatin, diazoacetyl-D,L-norleucine methyl ester/Cu^{2+} ions and 1,2-epoxy-3-(*p*-nitrophenoxy)propane. Furthermore, our recent site-directed mutagenesis studies[4-6] have demonstrated that two specific residues, the glutamic acid-110 (Glu B110) and the glutamine residue-24 (Gln B24), in the heavy chain are indispensable for the catalytic activity, different from the cases of aspartic peptidases which have a catalytic dyad of two aspartic acid residues.

To establish that these two residues (Glu B110 and Gln B24) are actually the catalytic residues, it is essential to elucidate the three-dimensional structure of the enzyme. Thus, we have solved the structure of AGP by X-ray crystallography to a 1.4-Å resolution. The results revealed that the enzyme has a unique structure, with an apparent partial two-fold symmetry, where the essential glutamic acid (Glu B110) and glutamine (Gln B24) residues identified by site-directed mutagenesis apparently form a catalytic dyad. Meanwhile, Fujinaga *et al.*[7] have reported the three-dimensional structure of scytalidoglutamic peptidase (SGP or eqolisin; *MEROPS* ID: G01.001; formerly called scytalidopepsin B) at 2.1-Å resolution, which is almost identical with the structure of AGP. This has accelerated publication of our results in a

[*1] Department of Biophysics and Biochemistry, Graduate School of Science, The University of Tokyo, 7-3-1 Hongo, Bunkyo-ku, Tokyo 113-0033, Japan.

[*2] Tokiwa Junior College, 1-430-1 Miwa, Mito, Ibaraki 310-8585, Japan.

[*3] Institute for Protein Research, Osaka University, 3-2 Yamadaoka, Suita, Osaka 565-0871, Japan.

[*4] Biophysics Division, National Cancer Center Research Institute, 5-1-1 Tsukiji, Chuo-ku, Tokyo 104-0045, Japan

[*5] Department of Applied Biological Chemistry, Graduate School of Agricultural and Life Sciences, The University of Tokyo, 1-1-1 Yayoi, Bunkyo-ku, Tokyo 113-8657, Japan.

[*6] School of Life Science, Tokyo University of Pharmacy and Life Science, 1432-1 Horinouchi, Hachioji, Tokyo 192-0392, Japan.

[†] Correspondence to: M. Tanokura.

Preliminary accounts of this study were presented at the 17th Congress of the International Union of Crystallography at Seattle, August 8-17th, 1996 (Abstract book, p. C-107) and at the 10th Annual Meeting of the Protein Society of Japan at Nagaoka, September 24-26th, 1998 (Abstract book, p. 179).

preliminary form.

Materials and methods. AGP was purified from the crude enzyme mixture obtained from the culture medium of *Aspergillus niger* var. *macrosporus*.[2] The crystals were grown from AGP (100 mg/ml) solution containing 1.4 M ammonium sulfate, 5% (v/v) dimethyl sulfoxide, 50 mM glycine buffer (pH 2.1) by hanging-drop vapor diffusion method essentially as described.[8),9)] The crystals belonged to space group $P2_12_12_1$ with unit cell dimensions of a = 55.1 Å, b = 70.7 Å and c = 38.3 Å, and had one molecule of AGP per asymmetric unit. All diffraction data were collected at BL6A in Photon Factory of High Energy Accelerator Research Organization (Tsukuba, Japan). The wavelength of X-rays used was 1.00 Å and the temperature was 10 °C. Data were processed using the HKL package[10] and the CCP4 suite[11] for the native protein data set, and WEIS[12] for the derivative data sets. The crystal structure was solved by a multiple isomorphous replacement with anomalous scattering (MIRAS) method using K_2PtCl_4 and $HgCl_2$ derivatives. The phases were calculated at 2.0-Å resolution with program MLPHARE[11] in the CCP4 program suite resulting in the figure of merit 0.57. Subsequently, density modification was applied by solvent flattering and histogram matching using program DM.[11] The initial model was constructed by using program O[13] and refined with program X-PLOR.[14] The current model contains the residues A1-32 (light chain) and B3-173 (heavy chain), 128 water molecules and 5 SO_4^{2-} ions. The crystallographic R-factor is 19.7% (free R-factor is 22.6%) for 29,266 reflections in the 10.0-1.4-Å resolution range. The root-mean square deviations from ideality were 0.008 Å for bond lengths and 1.669 degree for bond angles. All figures were produced by the program PyMOL.[15] Further experimental details will be published elsewhere, and the coordinates of AGP will soon be deposited in the Protein Data Bank.

Results and discussion. Figure 1 shows the overall structure of AGP in a ribbon model. The enzyme molecule was shown to be composed of eighteen β-strands and the loops connecting them, being entirely devoid of α-helix. This is consistent with the secondary structure prediction made previously from the circular dichroism spectroscopy.[16] There are two seven-stranded anti-parallel β-sheets (shown in green and red). These two sheets overlap with each other, thus forming a β-sandwich structure. This unique structure is essentially almost the same as that of SGP[7] and has not been reported previously in any other proteins. The C-terminus of the light chain is located close to the N-terminus of the heavy chain, consistent with the removal of the eleven residue intervening peptide during conversion of the proenzyme to the mature enzyme. The intervening peptide presumably protrudes from the rest of the protein molecule in the proenzyme so as to be easily susceptible to proteolysis at the two boundaries between the light chain C-terminus and the intervening peptide N-terminus and between the intervening peptide C-terminus and the heavy chain N-terminus. The function of this intervening peptide remains to be elucidated.

Interestingly, there appears to be a weak, but significant partial two-fold symmetry in the structure of AGP, as shown in Fig. 2. There is a water molecule sitting in the center of the protein molecule, toward which the putative catalytic residues, Glu B110 and Gln B24, extend their side chains from the symmetric β-strands 11 and 5, respectively (see also Fig. 3). These results might indicate the possibility that the AGP molecule was evolved by gene duplication and fusion as suggested more clearly for aspartic peptidases.[17]

Figure 3 shows the electron density map and deduced structure of part of AGP including the putative catalytic residues, Glu B110 and Gln B24. These residues are separated by a closest distance of 4.8 Å between atoms Glu B110 $O\varepsilon^1$ and Gln B24 $O\varepsilon^1$, forming a hydrogen bond net work with the three nearby water molecules and Trp B10 is hydrogen-bonded to Glu B110. These results are essentially the same as those obtained with SGP,[7] and therefore the mechanism of catalysis should be the same for both enzymes. The catalytic dyad composed of a glutamic acid and a glutamine is novel, and Fujinaga *et al.*[7] have proposed a mechanism for SGP in which the glutamic acid residue acts as a general base to accept a proton from one of the water molecule, which in turn attacks nucleophilically the carbonyl carbon of the scissile peptide bond of the substrate, while the glutamine residue stabilizes the transition state through hydrogen bonding. Further studies will be necessary, however, to strictly establish their catalytic mechanism.

Acknowledgments. We are most grateful to Prof. Setsuro Ebashi, M. J. A. (National Institute for Physiological Sciences, Okazaki) for his continued encouragement. Thanks are also due to Profs. Noriyoshi Sakabe and So Iwata (Institute of Materials Structure Science, High Energy Accelerator Research Organization, Tsukuba) for their helpful discussions. This study was supported in part by Grants-in-Aid for Scientific Research from the Ministry of Education, Culture, Sports, Science and Technology of Japan.

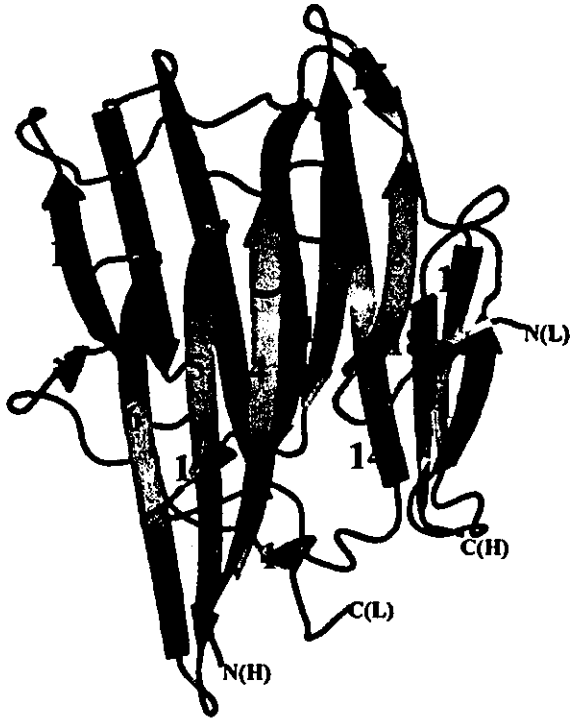

Fig. 1. Overall structure of AGP. The structure is shown in a ribbon model. The β-strands are numbered from the N-terminus to the C-terminus, starting from the light chain followed by the heavy chain. The first seven-stranded β-sheet and two extra short strands 7 and 13 are shown in green and the second seven-stranded β-sheet is in red. N(L) and C(L) indicate the N- and C-terminus, respectively, of the light chain, and N(H) and C(H) those of the heavy chain.

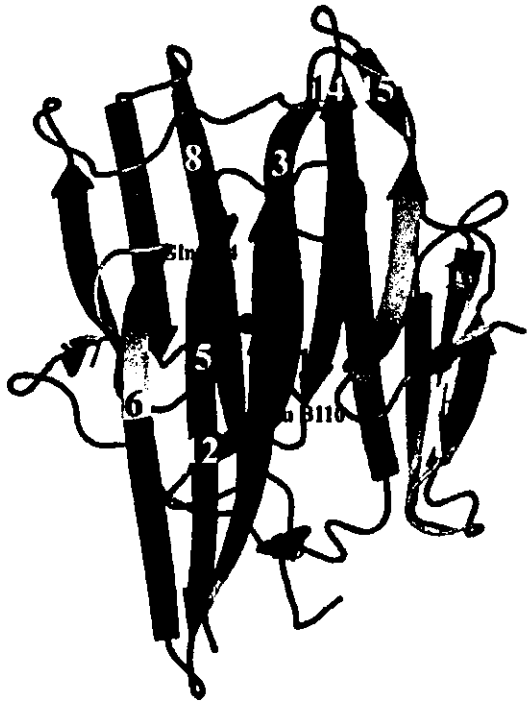

Fig. 2. Apparent two-fold symmetry in the AGP molecule. The side chains of Glu B110 and Gln B24 and a water molecule sitting in between (a black ball) are also shown. A two-fold symmetry axis positioned between the antiparallel strands 4 and 11 passes near the residue Glu B110. Each typical symmetric pair of β-strands is shown in the same color. The equivalent pairs are as follows: strand 3 corresponds to strand 8 (in red), strand 4 and the N-terminal part of strand 5 to strands 11, 12 and 13 (in green), the C-terminal part of strand 5 and the N-terminal part of strand 6 to the C-terminal part of strand 14 and strand 15 (in blue), the C-terminal part of strand 6 and strand 7 to strand 16 and the N-terminal part of strand 17 (in yellow). The gray parts do not have any relationships.

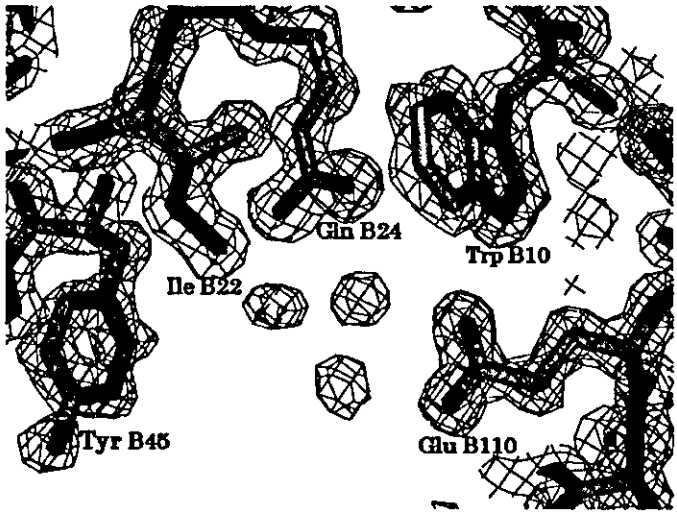

Fig. 3. Electron density map and the corresponding chemical structure of the putative active site region of AGP. $2F_o$-F_c map is contoured at 1sigma.

References

1) Takahashi, K. (2004) In Handbook of Proteolytic Enzymes, 2nd ed. (eds. Barrett, A. J., Rawlings, N. D., and Woessner, J. F.). Elsevier Academic Press, London, pp. 221-224.
2) Takahashi, K. (1995) Methods Enzymol. **248**, 146-155.
3) Takahashi, K., Inoue, H., Sakai, K., Kohama, T., Kitahara, S., Takashima, K., Tanji, M., Athauda, S. B. P., Takahashi, T., Akanuma, H. *et al.* (1991) J. Biol. Chem. **266**, 19480-19483.
4) Takahashi, K., Kagami, N., Huang, X.-P., Kojima, M., and Inoue, H. (1998) In Aspartic Proteinases. Retroviral and Cellular Enzymes (ed. James, M. N. G.). Plenum Press, New York, pp. 275-282.
5) Huang, X.-P., Kagami, N., Inoue, H., Kojima, M., Kimura, T., Makabe, O., Suzuki, K., and Takahashi, K. (2000) J. Biol. Chem. **275**, 26607-26614.
6) Yabuki, Y., Kubota, K., Kojima, M., Inoue, H., and Takahashi, K. (2004) FEBS Lett. **569**, 161-164.
7) Fujinaga, M., Cherney, M. M., Oyama, H., Oda, K., and James, M. N. G. (2004) Proc. Natl. Acad. Sci. USA **101**, 3364-3369.
8) Tanokura, M., Matsuzaki, H., Iwata, S., Nakagawa, A., Hamaya, T., Takizawa, T., and Takahashi, K. (1992) J. Mol. Biol. **23**, 373-375.
9) Sasaki, H., Tanokura, M., Muramatsu, T., Nakagawa, A., Iwata, S., Hamaya, T., Takizawa, T., Kono, T., and Takahashi, K. (1995) In Aspartic Proteinases: Structure, Function, Biology and Biomedical Implications (ed. Takahashi, K.). Plenum Press, New York, pp. 605-609.
10) Otwinowski, Z., and Minor, W. (1997) Methods Enzymol. **276**, 307-326.
11) Collaborative Computational Project, Number 4 (1994) Acta Cryst. **D50**, 760-763.
12) Higashi, T. (1989) J. Appl. Cryst. **22**, 9-18.
13) Jones, T. A., Zou, J. Y., Cowan, S. W., and Kjeldgaard, M. (1991) Acta Cryst. **A47**, 110-119.
14) Brünger, A. T. (1992) X-PLOR, Version 3.1, Yale Univ. Press, New Haven.
15) DeLano, W. L. (2002) The PyMOL Molecular Graphics System. DeLano Scientific, San Carlos.
16) Kojima, M., Tanokura, M., Maeda, M., Kimura, K., Amemiya, Y., Kihara, H., and Takahashi, K. (2000) Biochemistry **39**, 1364-1372.
17) Tang, J., James, M. N. G., Hsu, I. N., Jenkins, J. A., and Blundell, T. L. (1978) Nature **271**, 618-621.

(Received Oct. 30, 2004; accepted Nov. 12, 2004)

2P-386 Cleavage mode and specificity of *Escherichia coli* ATP-dependent Lon protease toward ribosomal S2 protein

°Wataru Nishii[1], Taichiro Suzuki[1], Tomonari Muramatsu[2], Kenji Takahashi[1] ([1]*Sch. of Life Sci., Tokyo Univ. of Pharmacy and Life Sci.*, [2]*GSC, RIKEN*)

wnishii@ls.toyaku.ac.jp

Recently, ATP-dependent Lon protease has been shown to degrade the ribosomal S2 protein in the presence of polyphosphate (polyP) in *Escherichia coli*. In this study, the cleavage mode and specificity were investigated *in vitro*. The enzyme was shown to degrade S2 in the presence of polyP 3 times faster than in the absence of polyP, while the cleavage specificities in the presence and absence of polyP were identical, indicating that polyP influenced not on the recognition but on the rate of cleavage of S2 by Lon. The enzyme produced 52 peptides with vaious sizes in a processive fassion. Cleavage occurred at 49 peptide bonds preferentially after hydrophobic residues, which were located in the regions rich in the secondary structure. Such a cleavage mechanism was similar to that toward other physiological substrates of Lon, such as SulA, CcdA and λN, and might contribute to accurate and complete degradation of the substrates.

Colloidal Nanoparticles: Electrokinetic Characterization

Kunio Furusawa
University of Tsukuba, Ibaraki, Japan

Hideo Matsumura
National Institute of Advanced Industrial Science and Technology, Tsukuba, Japan

INTRODUCTION

A charged colloidal particle suspended in an electrolyte solution is surrounded by a cloud of counterions. The set of the surface charges and countercharges is called the electrical double layer. The electrical double layer plays an essential role in various interfacial electrical phenomena on the particle surface and in the particle–particle interaction of colloid suspension.

Generally, it is almost impossible to measure the surface potential on colloid particles. However, we can measure the potential near the particle surface. It is called the zeta (ζ) potential. The zeta potential is the potential at the hydrodynamic slipping plane in the electrical double layer, hence its value is not precisely the same as that of making a stable suspension because the total interaction potential between two particles a bit distant from their surface is essential for a stable dispersion. The ζ-potential has been considered to provide useful information necessary for preparing stable colloidal suspensions in many application fields including food preparation, agriculture, pharmaceuticals, paper industry, ceramics, paints, coatings, photographic emulsions, etc. The concept of the zeta potential is also very important in such diverse processes as environmental transport of nutrients, sol–gel synthesis, mineral recovery, waste water treatment, corrosion, and many more.

OVERVIEW

These are several origins from which solid surfaces are charged: dissociation of chemical groups on the surface, preferential adsorption of cation or anion onto the surface, etc. The distribution of each ionic compound between the surface and the solution bulk is determined by the differences in the electrochemical potential of each compound between two phases: the solid (surface) phase and the solution phase. Therefore the composition of the solution is an important factor that determines surface potentials. When H^+ is the potential-determining ion, we can change the amount of surface charge by changing the pH of the solution. It is important to know the position of the isoelectrical point (IEP) (i.e., the pH value at which the particles have zero ζ-potential). At the IEP, there are no repulsive forces and the particles are strongly aggregated because of the attractive van der Waals forces. In many cases, the stable colloidal particle dispersion is desired, so the colloidal suspensions are designed such that the pH of the suspension is well away from the IEP. The IEP data for a number of colloids of various compositions have been reported.[1] Table 1 lists the IEP for some typical dispersions.

If colloid particles are brought to a concentrated situation through some engineering processes, it is not certain if the surface charges, and hence surface potential, hold the same values as those in diluted dispersions. It must be measured experimentally, and several methods have been explored in recent years.

Here, we briefly describe experimental methods of the measurements of ζ-potential for the diluted and the concentrated particle systems, and how the control of zeta potential is useful for preparing composite particle systems in the last part of this report. The fundamentals of electrokinetics in colloidal systems have been described in numerous books in recent years.[1–3]

MEASUREMENTS OF ζ OF PARTICLES IN DILUTED SUSPENSION

Regular Method by Electrophoresis

The historical prominence of ζ-potential has been because of its experimental accessibility via measurement of the electrophoretic mobility μ. Electrophoretic mobility is the velocity of the colloid particle v per unit field strength E:

$$v = \mu E \tag{1}$$

Dekker Encyclopedia of Nanoscience and Nanotechnology
DOI: 10.1081/E-ENN 120009085

Table 1 Isoelectric points

Compound	IEP (pH)
α-AlOOH	9.4
γ-AlOOH	5.5–7.5
α-$Al(OH)_3$	5.0–5.2
γ-$Al(OH)_3$	9.3
CdO	10.4
Co_3O_4	5.5
$Co(OH)_2$	10.5
α-Fe_2O_3	8.3
βFe_2O_3	6.7–8.0
$Mg(OH)_2$	12
MnO, MnO_2	6
NiO	9.5
SiO_2	1.8–2.5
SnO_2	4.5
TiO_2	6
ZrO_2	4

where ζ is related with mobility by the equation from von Smoluchowski:[4]

$$\mu = \varepsilon\zeta/\eta \tag{2}$$

where ε or η are the permittivity or viscosity of the medium, respectively. In regular electrophoretic apparatus, we utilize a narrow capillary cell of cylindrical or rectangular shape. The migration velocity of the particles is measured by optical microscopy for larger-sized particles, or by observation of Doppler shift of laser light scattering signal for smaller particles. However, the capillary cell walls also bear electrical charges and hence have electrical double layers. Therefore the application of electrical fields causes the movement of charged liquid medium in the double layer, which is called electroosmosis. The electrophoretic migration of colloid particles is always superimposed on the electroosmotic liquid flow from the cell wall. The closed sample cell causes a back liquid flow through the generation of hydrostatic pressure gradient. At equilibrium, there are two positions where the liquid flow has zero velocity. These are called the stationary levels. Thus we can observe the true electromigration velocity of colloid particles at the stationary levels. Von Smoluchowski[4] showed the profile of electroosmotic flow velocity (U_{osm}) for a cylindrical cell:

$$U_{osm} = U_0(h^2/b^2 - 1) \tag{3}$$

and for a flat cell, which has an infinitely long width:

$$U_{osm} = U_0/2(3h^2/b^2 - 1) \tag{4}$$

where h is the distance from the cell center in the direction of cell thickness, b is the half-thickness of the cell, and U_0 is the electroosmotic flow at the cell wall ($h=b$). The stationary levels are located at a distance from the cell center to each side by the quantity $h=b/\sqrt{2}$ for the cylindrical cell, or $h=b/\sqrt{3}$ for the flat cell. Komagata[5] showed a more practically useful equation for a rectangular cell, which has a thickness of $2b$ and a width of $2w$ ($b<w$); the stationary level is located at a distance from the cell center to each side by the quantity $h=b\sqrt{(1/3(1 + 384b/\pi^5 w))}$. The traditional measurements of zeta potentials of particles are conducted at these stationary levels.

Electrophoretic Measurements Using a Standard Sample

The profile of electroosmotic flow is parabolical. Thus the velocity gradient of the liquid at the stationary levels is usually large and the observed velocity of the particles changes rapidly with cell depth. It causes substantial errors in electrophoretic mobility measurements from the wrong setting of observing points. However, if the electrophoretic measurements can be carried out by using a reference sample as a standard, the electrophoretic mobility of the unknown sample can be determined at any cell depth by subtracting the mobility of the reference particles at the same level, because the velocity of electroosmotic liquid flow induced by the cell wall has the same value under the same experimental conditions. Therefore one can obtain real electrophoretic mobility rather accurately by measuring the velocity at the cell center, where the velocity gradient is zero.

The apparent electrophoretic mobility (U_{app}) of an unknown colloid sample is always the sum of two contributions, one of which is the real electrophoretic mobility (U_{el}) and the other is the liquid flow velocity induced by the electroosmotic effect (U_{osm}) of the cell wall, which changes as a parabolical function of the cell depth:

$$U_{app} = U_{el} + U_{osm} \tag{5}$$

Similarly, the apparent velocity of the reference sample (U_{app}') was also indicated by the sum of the real electrophoretic mobility (U_{el}') and the electroosmotic flow velocity (U_{osm}'), that is,

$$U'_{app} = U'_{el} + U'_{osm} \tag{6}$$

Under the same experimental conditions, using a finite electrophoretic cell ($U_{osm}=U_{osm}'$), the following relationship holds from Eqs. 5 and 6:

$$U_{el} - U'_{el} = U_{app} - U'_{app} \tag{7}$$

If U_{el}' is known exactly, the U_{el} value of the unknown sample can be determined from the difference between

MARCEL DEKKER, INC.
270 Madison Avenue, New York, New York 10016